



Phase transitions and magnetocaloric effect in $\text{Mn}_3\text{Cu}_{0.89}\text{N}_{0.96}$

Jun Yan^a, Ying Sun^{a,*}, Hui Wu^{b,c}, Qingzhen Huang^b, Cong Wang^{a,*}, Zaixing Shi^a,
Sihao Deng^a, Kewen Shi^a, Huiqing Lu^a, Lihua Chu^a

^a Center for Condensed Matter and Materials Physics, Department of Physics, Beihang University, Beijing 100191, People's Republic of China

^b NIST Center for Neutron Research, NIST, Gaithersburg, MD 20899-6102, USA

^c Department of Materials Science and Engineering, University of Maryland, College Park, MD 20742, USA

Received 5 March 2014; received in revised form 1 April 2014; accepted 4 April 2014

Abstract

We report a large magnetic entropy change observed in the antiperovskite $\text{Mn}_3\text{Cu}_{0.89}\text{N}_{0.96}$. Based on the heat flow peak measured by differential scanning calorimetry, the total entropy change according to the structural transition (tetragonal to cubic) was calculated to be $\sim 60 \text{ J kg}^{-1} \text{ K}^{-1}$ while the magnetic entropy change accounts for $\sim 22.5\%$ of the total entropy under a 50 kOe magnetic field at 145 K. To clarify the origin of the magnetic entropy change, we managed to control the structure transition using a magnetic field. It was found that the magnetic entropy change originates from the transformation from antiferromagnetic (AFM) to ferromagnetic (FM) as well as from the phase transition from cubic to tetragonal under the magnetic field. In the tetragonal phase, a magnetic field can drive the AFM component to transform gradually to the FM component. The magnetic field can also change the phase fraction in the tetragonal and cubic two-phase coexistence region, a similar behavior to that induced by temperature. In the current system, only 5.4% of the cubic phase transforms to the tetragonal phase at 5 Tesla (T), indicating there is still much latent entropy in $\text{Mn}_3\text{Cu}_{0.89}\text{N}_{0.96}$.

© 2014 Acta Materialia Inc. Published by Elsevier Ltd. All rights reserved.

Keywords: Entropy; Magnetic; Phase transition; Neutron diffraction

1. Introduction

Materials with a large magnetocaloric effect (MCE) have attracted much attention in recent years. Most of these materials with large MCE contain expensive and sometimes toxic rare-earth elements [1]. Development of low-cost and innocuous materials with large MCE is therefore critical for practical applications.

Some antiperovskite compounds with large MCE have potential for magnetocooling technology. Mn_3GaC has been found to undergo an abrupt first-order transition from antiferromagnetic (AFM) to ferromagnetic (FM) at $\sim 165 \text{ K}$, and this transition can be induced by a magnetic

field [2–5]. A large magnetic entropy change of $15 \text{ J kg}^{-1} \text{ K}^{-1}$ below 20 kOe was estimated from the Maxwell equation for the isothermal magnetization curves of Mn_3GaC [2,3]. Carbon content was found to be capable of altering the magnetic state of Mn_3GaC and influencing the entropy variation of the phase transition [6–8]. It was reported that by introducing 22% vacancies at carbon positions, the magnetic entropy change can be reduced to $3.7 \text{ J kg}^{-1} \text{ K}^{-1}$ under a magnetic field of 50 kOe in $\text{Mn}_3\text{GaC}_{0.78}$ [7]. In addition, substitution of Co for Mn in Mn_3GaC can lower the first-order magnetic transition temperature from 160 to 100 K without significant loss of MCE. As a result, Co doping broadens the region of the large MCE in $\text{Mn}_{3-x}\text{Co}_x\text{GaC}$ [9]. In order to generate large magnetic entropy, a sharp change of magnetization is necessary. Mn_3CuN undergoes a first-order structural transition from cubic to tetragonal accompanied by a paramagnetic (PM)

* Corresponding authors.

E-mail addresses: sunying@buaa.edu.cn (Y. Sun), congwang@buaa.edu.cn (C. Wang).

to ferrimagnetic (FIM) magnetic transition [6,10]. Mn_3SnC has a similar magnetic structure to Mn_3CuN [6]. Wang et al. reported that Mn_3SnC has magnetic entropy $-\Delta S_m = 80.69 \text{ mJ cm}^{-3} \text{ K}^{-1}$ (corresponding to $10.37 \text{ J kg}^{-1} \text{ K}^{-1}$) and $-\Delta S_m = 133 \text{ mJ cm}^{-3} \text{ K}^{-1}$ (corresponding to $17 \text{ J kg}^{-1} \text{ K}^{-1}$) at 20 kOe and 48 kOe, respectively [11]. The structure variation and the resulting giant magnetostriction property of Mn_3SbN are analogous to those of Mn_3CuN [12]. In Mn_3SbN , the total entropy of the phase transition process is $10.2 \text{ J mol}^{-1} \text{ K}^{-1}$ (corresponding to $34.93 \text{ J kg}^{-1} \text{ K}^{-1}$) and the magnetic entropy induced by a magnetic field of 50 kOe is $2.1 \text{ J mol}^{-1} \text{ K}^{-1}$ (corresponding to $7.19 \text{ J kg}^{-1} \text{ K}^{-1}$), hence most of the entropy originates from lattice entropy [13]. To the best of our knowledge, there is no report so far on the total and magnetic entropy of Mn_3CuN . According to Ref. [6], the Mn_2 atom in Fig. 1b has an AFM moment of $2.85 \mu_B$ and a FM moment of $0.2 (0.15) \mu_B$, the Mn_1 atom in Fig. 1b has a FM moment of $0.65 (0.15) \mu_B$ at 4.2 K in Mn_3CuN , from which it can be seen that Mn_3CuN displays weak FM component for neutron detection. Hence we have attempted to prepare $\text{Mn}_3\text{Cu}_x\text{N}_y$, so as to obtain a large MCE. It would be of great interest to investigate the entropy in $\text{Mn}_3\text{Cu}_x\text{N}_y$ due to its intriguing

coupled structural and magnetic phase transitions and the possible resultant MCE.

A variety of fascinating physical properties related to its magnetic, electronic and lattice properties have been found in $\text{Mn}_3\text{Cu}_x\text{A}_{1-x}\text{N}_y$ (where A is a doping element). Chi et al. reported a near-zero temperature coefficient of resistivity (NZ-TCR) in Mn_3CuN and found that the TCR was $\sim 46 \text{ ppm K}^{-1}$ at about room temperature [14] and could be improved by partial substitution of Cu by Ni or Ag [15,16]. Negative thermal expansion (NTE) behaviors were found in some Mn-based antiperovskites, such as Mn_3AN (A = Cu, Zn, Ga), and partial substitution of A by Ge can induce and adjust the temperature range of the NTE property [17–21]. The magnetic–lattice coupling can be adjusted by inducing vacancies in some antiperovskite structures [22,23]. Furthermore, anisotropic magnetostriction behavior was found in Mn_3CuN_x [24,25]. All these properties were related to electronic entropy, lattice entropy and magnetic entropy.

In this paper, we use differential scanning calorimetry (DSC) and a superconducting quantum interference device (SQUID) magnetometer to study the entropy changes of the phase transitions in $\text{Mn}_3\text{Cu}_{0.89}\text{N}_{0.96}$. We found that the magnetic entropy in a magnetic field of 50 kOe is much less than the total transitional entropy. To understand such a large entropy and reveal its mechanism, we used neutron powder diffraction (NPD) to study the crystal and magnetic structures, and the structural transitions in $\text{Mn}_3\text{Cu}_{0.89}\text{N}_{0.96}$ under magnetic fields, and to clarify the correlations between the structure and the magnetic and entropy changes.

2. Experiment

A polycrystalline sample of $\text{Mn}_3\text{Cu}_{0.89}\text{N}_{0.96}$ was synthesized by a solid-state reaction method in vacuum (10^{-5} Pa) using Mn_2N_x and Cu (purity 99.99%) as starting materials [23]. Crystal and magnetic structures and their phase transitions were determined by NPD and Rietveld refinement with the General Structure Analysis System (GSAS) program [26]. The NPD data were collected at the BT-1 high-resolution neutron powder diffractometer at NIST Center for Neutron Research (NCNR), using a Cu (311) monochromator with wavelength of 1.5403 \AA . The intensities were measured with a scanning step size of 0.05° in the 2θ range $3\text{--}165^\circ$. Data were collected in the $6\text{--}300 \text{ K}$ temperature range, and under a magnetic field of up to 6 T (produced by a vertical superconductor magnet) to study the effect of magnetic field on the crystal and magnetic structures. The sample was sealed in a cylindrical vanadium container filled with He exchange gas. The neutron scattering amplitudes used in refinements were -0.375 , 0.772 and $0.936 (\times 10^{-12} \text{ cm})$ for Mn, Cu and N, respectively.

DSC was used to measure the crystal and/or magnetic phase transformation and to calculate the entropy change. The temperature dependence of magnetization was

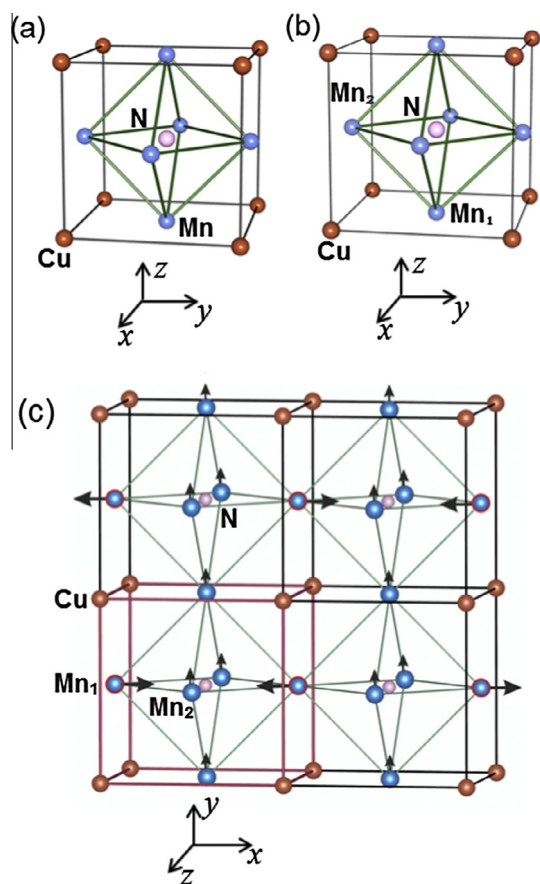


Fig. 1. Crystal structures and magnetic structure of $\text{Mn}_3\text{Cu}_{0.89}\text{N}_{0.96}$: (a) cubic structure with $Pm\bar{3}m$ symmetry; (b) tetragonal structure with $P4/mmm$ symmetry; (c) orthorhombic magnetic structure model with $P1$ symmetry at 6 K ($a_M = 2c_N$, $b_M = 2a_N$, $c_M = b_N$).

measured between 10 and 300 K under magnetic field of 500 Oe using a SQUID magnetometer. The measurement was conducted under field cooling conditions. A set of magnetization isotherms ($M-H$) at selected temperatures near the phase transition temperature were measured and the magnetic entropy change was calculated using the Maxwell equation.

3. Results and discussion

3.1. Crystal and magnetic structures

The $Mn_3Cu_{0.89}N_{0.96}$ sample adopts a cubic structure with space group $Pm\bar{3}m$ above 152 K and a tetragonal structure with $P4/mmm$ symmetry below 143 K. A two-phase coexistence region was found between 152 and 143 K. Fig. 1a and b show the cubic structure and tetragonal structure, respectively. Fig. 1c illustrates the magnetic structure model of $Mn_3Cu_{0.89}N_{0.96}$. It exhibits an orthorhombic symmetry with $a_M = 2c_N$, $b_M = 2a_N$, $c_M = b_N$, where a_M , b_M , c_M are magnetic lattice parameters and a_N , b_N , c_N are nuclear lattice parameters. The magnetic structure refinement revealed that the Mn moments show an AFM component of $3.65(2) \mu_B$ on the $c_M = 0.5$ plane, and a FM component of $0.91(0.04) \mu_B$ parallel to the y axis on the $a_M = 0.25$ and 0.75 planes at 6 K. The magnetic structure of $Mn_3Cu_{0.89}N_{0.96}$ thus shows a ferrimagnetic (FIM) state.

Fig. 2a and b shows the effect of temperature on the crystal and magnetic transition. The variation of the

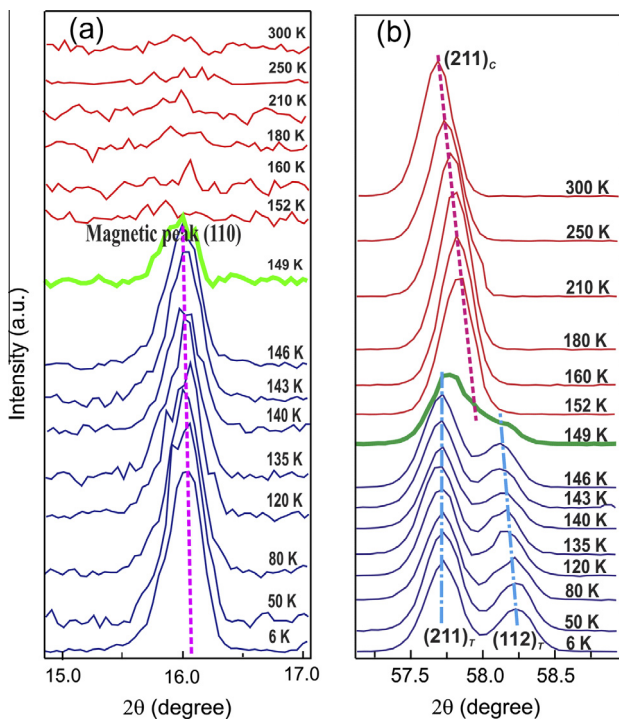


Fig. 2. Temperature dependence of the intensities of (a) the magnetic peak (110) and (b) the nuclear peak (211) of $Mn_3Cu_{0.89}N_{0.96}$.

nuclear peak (211) and the magnetic peak (110) can characterize the crystal and magnetic structure evolutions as a function of temperature. The nuclear peak (211) splits into two peaks (211) and (112), which indicates a phase transition from cubic to tetragonal structure. Meantime, the magnetic peak (110) intensity gradually increases with decreasing temperature. The lattice parameters increase along the a and b axes and decrease along the c axis with decreasing temperature. According to the NPD results, $Mn_3Cu_{0.89}N_{0.96}$ exhibits a FIM structure at low temperature as shown in Fig. 1c. Studying the crystal and magnetic evolutions with temperature as shown in Fig. 2, we can see that the structural transition is exactly consistent with the magnetic ordering on cooling, and the cubic and the tetragonal phases correspond to the PM and FIM states, respectively.

3.2. DSC measurements

We used DSC to measure the phase transitions and the latent heat of the $Mn_3Cu_{0.89}N_{0.96}$ sample, and to calculate the entropy changes associated with the phase transitions. The temperature dependence of the heat flow and entropy change in the cooling and warming processes are shown in Fig. 3a and b, respectively. Sharp exothermic and

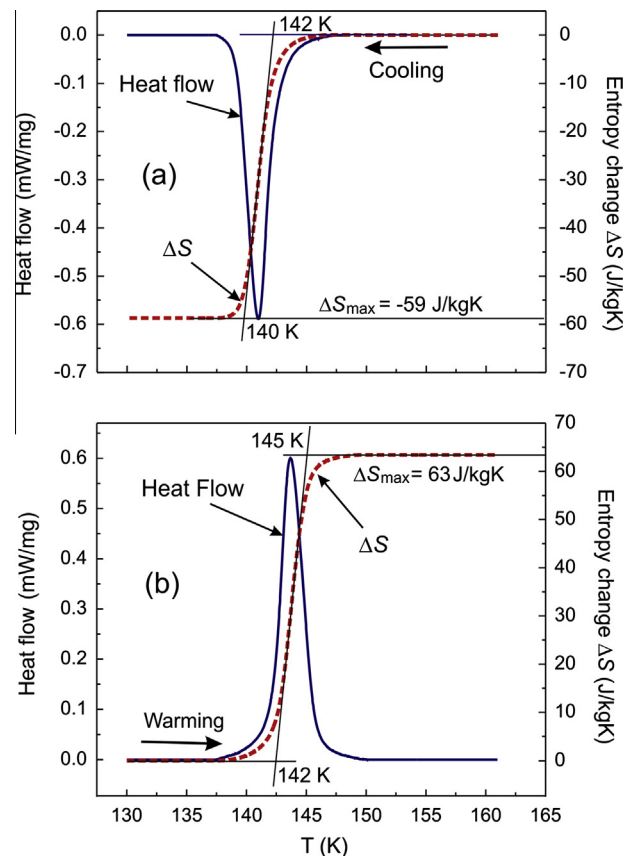


Fig. 3. Temperature dependence of the heat flow (left axis) and entropy change (right axis) for $Mn_3Cu_{0.89}N_{0.96}$: (a) cooling, with $\Delta S_{\max} = -59 \text{ J kg}^{-1} \text{ K}^{-1}$ (exothermic process); (b) warming, with $\Delta S_{\max} = 63.45 \text{ J kg}^{-1} \text{ K}^{-1}$ (endothermic process).

endothermic peaks associated with the transitions were observed in the cooling and warming processes, respectively. The transition temperature was observed to be 142 K (onset) upon cooling and warming without thermal hysteresis. The total entropy changes (ΔS) can be estimated using the following equation:

$$\Delta S = S_{T_2} - S_{T_1} = \int_{T_1}^{T_2} \frac{C_p}{T} dT = \int_{T_1}^{T_2} \frac{dH}{dt} \cdot \frac{dt}{dT} \cdot \frac{1}{T} dT, \quad (1)$$

where the C_p , T , H , t and $\frac{dH}{dt}$ denote heat capacity at constant pressure, temperature, enthalpy, time and the heat flow. The maximum total entropy changes (ΔS_{\max}) are $59 \text{ J kg}^{-1} \text{ K}^{-1}$ (exothermic process) and $63 \text{ J kg}^{-1} \text{ K}^{-1}$ (endothermic process) upon cooling and warming, respectively.

3.3. Magnetization measurements

The entropy change normally consists of three parts: lattice entropy, electronic entropy and magnetic entropy. The magnetic measurements were performed to deduce the magnetic entropy. Fig. 4 displays the temperature dependence of the magnetization and inverse susceptibility of $\text{Mn}_3\text{Cu}_{0.89}\text{N}_{0.96}$ sample. The onset temperature of the transition (T_c) from the PM to the FM state is 147.7 K, slightly lower than the $T_c = 150 \text{ K}$ reported in Mn_3CuN [14]. As shown in Fig. 4, when the temperature is much higher than the T_c , the variation of the inverse magnetic susceptibility $1/\chi(T)$ with temperature follows the Curie–Weiss law. However, the Curie–Weiss law fails to describe the susceptibility in the vicinity of T_c . The $1/\chi(T)$ curve shows characteristics of the FIM state. Previous neutron diffraction measurement revealed that the ground state of Mn_3CuN exhibited FIM characteristics which consisted of AFM and FM components [6]. Based on the M – T and $1/\chi(T)$ curves in the present work, we confirmed that in $\text{Mn}_3\text{Cu}_{0.89}\text{N}_{0.96}$ there is an FM component and a sharp magnetic transition upon cooling, both of which are necessary for a large magnetic entropy change. A magnetic

entropy change can be derived from the magnetization measurements using the Maxwell relation.

Fig. 5a presents the magnetization isotherms of the sample at selected temperatures near T_c . The isotherms were measured with increasing and decreasing magnetic field (loop history 0–50–0 kOe). The magnetization suddenly decreased with increasing temperature from 144 to 146 K, indicating a large entropy change. Based on these M – H curves, the magnetic entropy change can be evaluated via the Maxwell equation [27]:

$$\begin{aligned} \Delta S_M(T, H) &= S_M(T, H) - S_M(T, 0) \\ &= \int_0^H \left(\frac{\partial M(T, H)}{\partial T} \right)_H dH, \end{aligned} \quad (2)$$

where $\Delta S_M(T, H)$, T , H and M denote magnetic entropy change, temperature, magnetic field and mass magnetization, respectively. The temperature dependence of ΔS_M calculated from Eq. (2) with fields of 5, 10, 20, 30, 40 and 50 kOe is shown in Fig. 5b. The maximum value of $-\Delta S_M$ was determined to be $13.52 \text{ J kg}^{-1} \text{ K}^{-1}$ at 50 kOe near T_c , much smaller than the total entropy changes of $\sim 60 \text{ J kg}^{-1} \text{ K}^{-1}$ obtained from the DSC measurement:

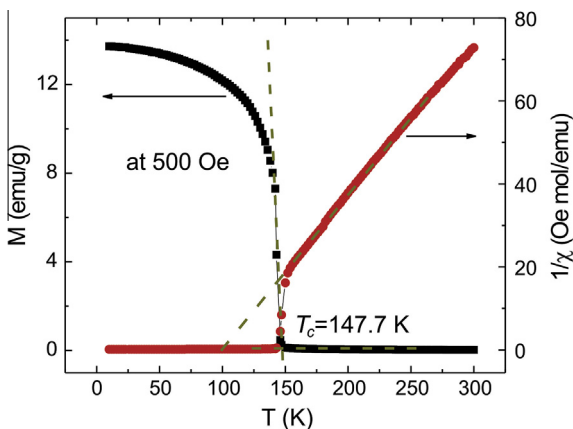


Fig. 4. Temperature dependence of the magnetization, M – T , at $H = 500 \text{ Oe}$ (left axis) and the inverse susceptibility (right axis).

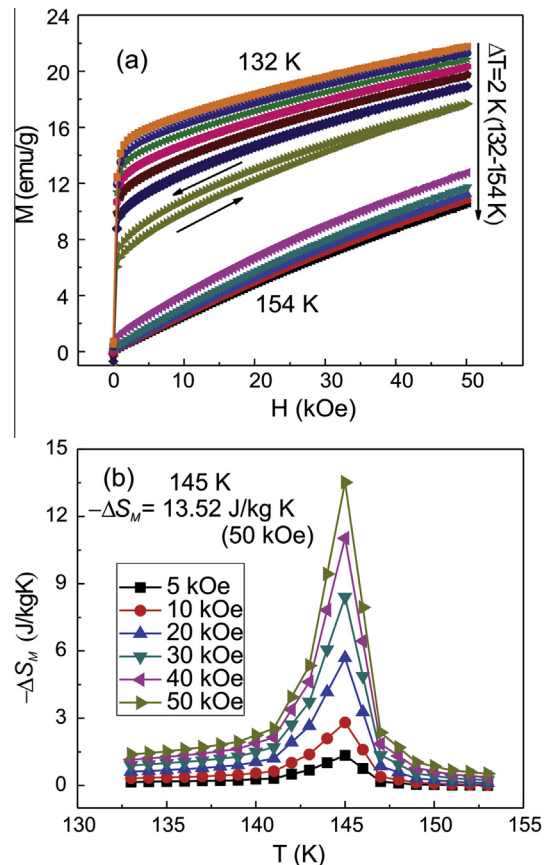


Fig. 5. (a) Magnetization isotherms of $\text{Mn}_3\text{Cu}_{0.89}\text{N}_{0.96}$ at various temperatures in the presence of external magnetic fields up to 50 kOe. (b) Magnetic field-induced isothermal entropy change as a function of temperature under various applied magnetic fields.

$$RCP = \left| \int_{T_1}^{T_2} \Delta S_M(T) dT \right| \approx \left| \Delta S_M^{\max} \delta T_{FWHM} \right| \quad (3)$$

where RCP is refrigeration capacity, T_1 is the initial temperature and T_2 is the final temperature, $\Delta S_M(T)$ is the magnetic entropy change as a function of temperature, ΔS_M^{\max} is the maximum magnetic entropy change and δT_{FWHM} is the full width at half maximum. According to Eq. (3) [28], the relative cooling power (RCP) is 38.94 J kg^{-1} . In addition, from the M–H loops, there is only a small hysteresis at 146 K, suggesting small hysteresis loss of $\text{Mn}_3\text{Cu}_{0.89}\text{N}_{0.96}$ compound for practical applications in magnetic refrigeration.

3.4. Relationship between the structure transition and entropy change

From the NPD study on $\text{Mn}_3\text{Cu}_{0.89}\text{N}_{0.96}$, $\text{Mn}_3\text{Cu}_{0.89}\text{N}_{0.96}$ undergoes a structure transition from cubic to tetragonal at 143 K accompanied by a magnetic ordering on cooling. The structure distortion can be explained by the Jahn–Teller effect [6,29]. The Jahn–Teller distortion (cubic to tetragonal) removes the degeneracy of the hybridization narrow band between Mn 3*d* and N 2*p* in $\text{Mn}_3\text{Cu}_{0.89}\text{N}_{0.96}$. The process is related to the electronic transfer between the large conduction band and the narrow band, thus is related to the resistivity [6,32]. Fig. 6 shows the temperature dependence of resistivity for $\text{Mn}_3\text{Cu}_{0.89}\text{N}_{0.96}$. There is an anomalous increase in resistivity around the transition temperature T_c with decreasing temperature. The sudden change in the resistivity leads to the electronic entropy change. As such electron-transfer originated resistivity stems from Jahn–Teller structural distortion, the electronic entropy change is therefore believed to be induced by structure distortion in $\text{Mn}_3\text{Cu}_{0.89}\text{N}_{0.96}$.

To further elucidate the relationship between the total entropy change and the structure transition, we compare the total entropy change with the variation of nuclear peak (211) as a function of temperature. As shown in Fig. 7, the variation of the integrated intensity of peak (211) indicates the structural transition. With increasing temperature, the

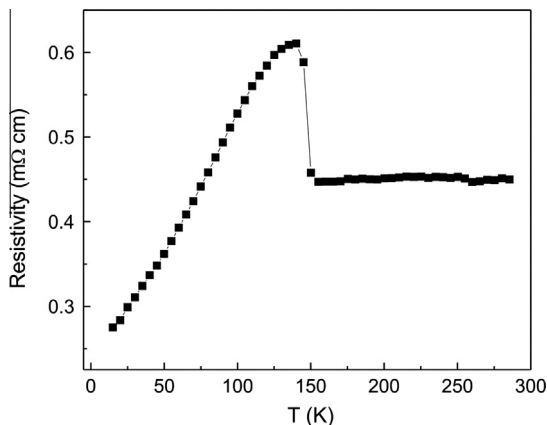


Fig. 6. Temperature dependence of the resistivity for $\text{Mn}_3\text{Cu}_{0.89}\text{N}_{0.96}$.

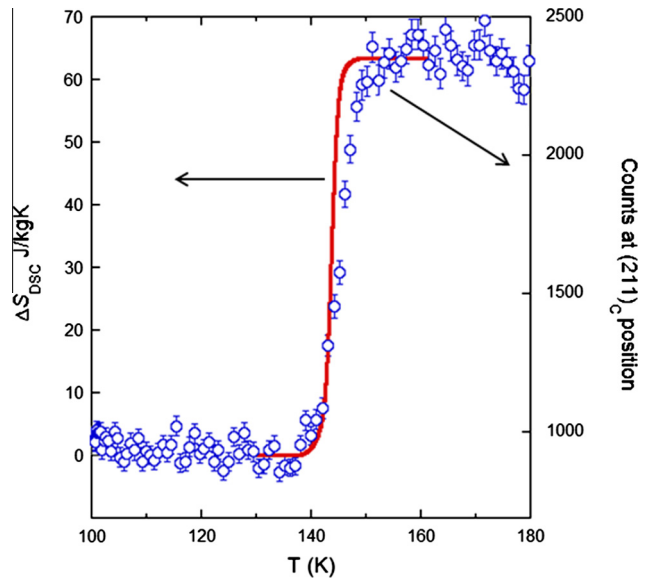


Fig. 7. Temperature dependence of entropy change (left axis) and the intensity of nuclear peak (211) (right axis) of $\text{Mn}_3\text{Cu}_{0.89}\text{N}_{0.96}$ upon warming.

tetragonal structure gradually transforms to cubic structure and the intensity of peak (211) increases. The transition temperature region and the variation in entropy nearly coincide with the intensity of peak (211) with almost the same onset temperature. The small deviations observed can be ascribed to system errors between the different measuring instruments. Therefore, it can be concluded that the total entropy change is directly related to the structural and magnetic transitions. The cubic phase corresponds to the PM state and the tetragonal phase corresponds to the FIM state.

3.5. Magnetic field effect

In order to understand the mechanism of the MCE in a magnetocaloric material, it is critical to clarify the effects of magnetic field on magnetic and structural transition. It had been reported that a transition from AFM state to FM state can be induced by applying a magnetic field in Mn_3GaC [4,5]. Therefore, applying an external magnet field would help trigger the phase transition and determine the origin of the MCE in $\text{Mn}_3\text{Cu}_{0.89}\text{N}_{0.96}$.

From the literature, it appears that the application of a magnetic field does not affect the profiles of the X-ray diffraction patterns of Mn_3CuN when it exists as a tetragonal phase at 120 K or as a cubic phase at 150 K under a magnetic field of 5 T [24]. In addition, a small magnetocrystalline anisotropy was observed in Mn_3CuN [30]; therefore, if the magnetocrystalline force is large enough to fix the magnetic moments along the magnetization easy axis in a field, the component of the effective field on each grain would be widely distributed and more energy is then needed to excite the state. On the other hand, it is well known that triggering a structural phase transition needs

less energy at a temperature near T_c than at a temperature far from T_c . For example, at the first-order transition temperature of 165 K in Mn_3GaC , a magnetic field of only 1 T can induce the transition from the AFM to the FM state. However, at 50 K, a magnetic field of as large as 17 T is needed to induce this transition [31].

From those observations, we choose a tetragonal phase region (e.g. 140 K) and a two-phase coexistence region (e.g. 144 K, with 18.5% tetragonal phase and 81.5% cubic phase) to apply magnetic fields for an easier transition induction.

Figs. 8 and 9 show the variations of the lattice, magnetic and phase fractions for $\text{Mn}_3\text{Cu}_{0.9}\text{C}_{0.96}$ under a magnetic field at 140 and 144 K, respectively. The magnetic field dependence of these parameters can be fitted with a linear equation. For the lattice parameters:

$$a_H = a(0) + \beta_1 B(T), \text{ or } c_H = c(0) + \beta_2 B(T). \quad (4)$$

Here a_H and c_H are the lattice parameters along the a axis and the c axis under a magnetic field, respectively, $a(0)$ and $c(0)$ are the lattice parameters without a magnetic field. B is the magnetic field in Tesla (T). β_1 and β_2 are scaling factors

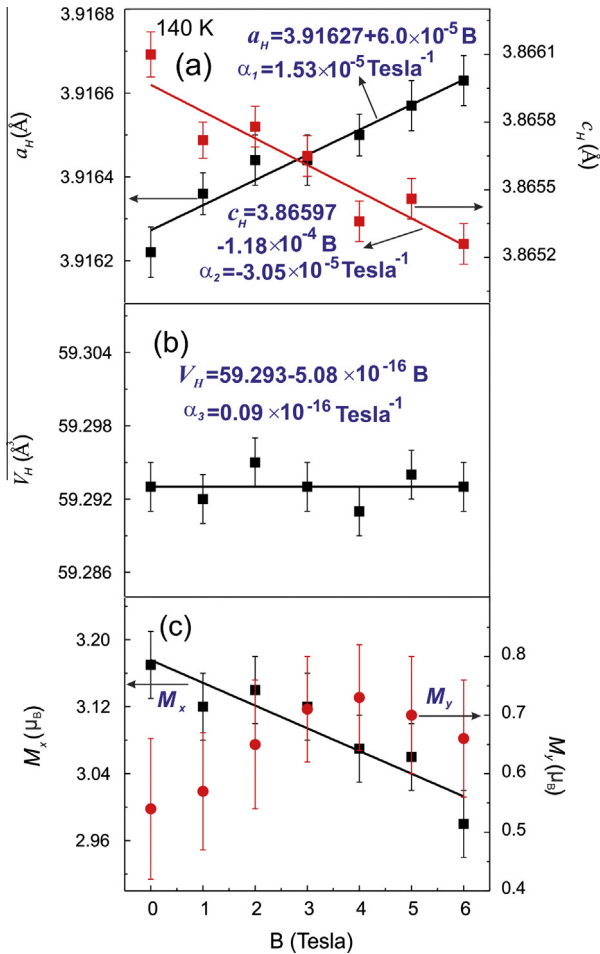


Fig. 8. Variations of (a) the lattice parameters a_H and c_H , (b) the tetragonal unit cell volume V_H , and (c) the antiferromagnetic moment M_x (left axis) and the ferromagnetic moment M_y (right axis) of $\text{Mn}_3\text{Cu}_{0.89}\text{N}_{0.96}$ under various magnetic fields at 140 K.

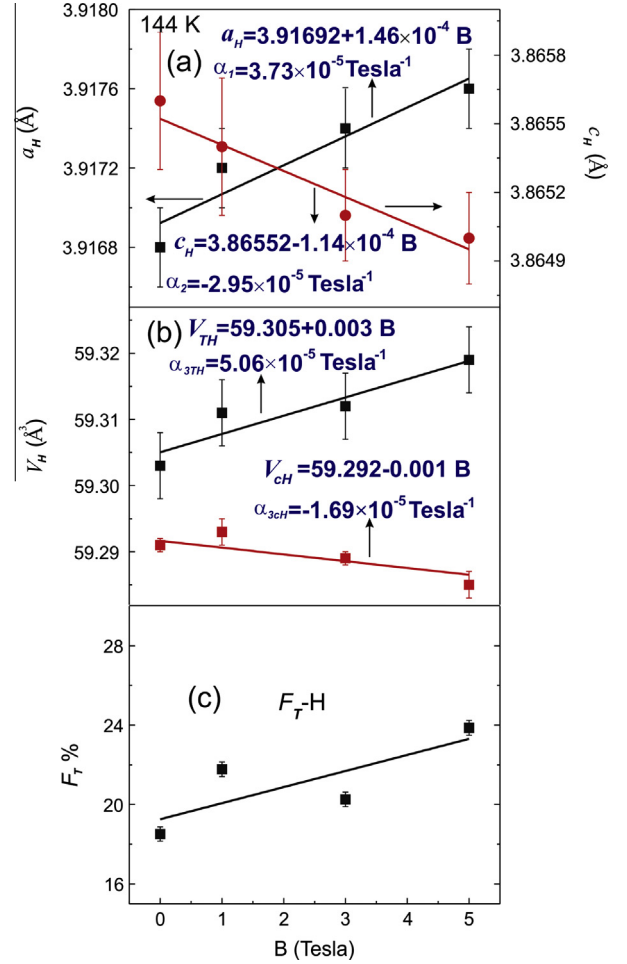


Fig. 9. Variations of (a) the lattice parameters a_H and c_H , and (b) the tetragonal cell volume V_{TH} and cubic cell volume V_{cH} , and (c) the tetragonal phase fraction F_T in $\text{Mn}_3\text{Cu}_{0.89}\text{N}_{0.96}$ under a magnetic field at 144 K.

($\beta_1 = \Delta a/\Delta B$, $\beta_2 = \Delta c/\Delta B$), and Δa and Δc are the variations of the corresponding lattice parameters, respectively. ΔB is the variation of magnetic field. $\alpha_1 = \beta_1/a(0)$ or $\alpha_2 = \beta_2/c(0)$ is the linear lattice expansion or contraction coefficient induced by a magnetic field. For the volume:

$$V_H = V(0) + \beta_3 B(T). \quad (5)$$

Here V_H is the volume at a magnetic field measured in Tesla, and $V(0)$ is the volume without the magnetic field. $\beta_3 = \Delta V/\Delta B$, ΔV and ΔB are the variations of the volume and the magnetic field, respectively. $\alpha_3 = \beta_3/V(0)$ is the linear volume expansion or contraction coefficient induced by a magnetic field.

3.5.1. Magnetic field effects in the tetragonal phase region (140 K)

Fig. 8a shows that the $\text{Mn}_3\text{Cu}_{0.89}\text{N}_{0.96}$ unit cell expands along both the a axis and the b axis but contracts along the c axis with increasing magnetic field. The linear expansion coefficient of the a axis and the shrinkage coefficient of the c axis induced by the magnetic field are 1.53×10^{-5} and

$-3.05 \times 10^{-5} \text{ T}^{-1}$ at 140 K, respectively. The lattice expansion along the a and b axes offsets the lattice contraction along the c axis; therefore, there is no net cell volume change with increasing magnetic field at 140 K as shown in Fig. 8b. The ratio of c_T/a_T ($c_T < a_T$, $c_T/a_T < 1$) decreases with increasing magnetic field, indicating that the lattice distortion is increasing. Hence, it is difficult to promote the structural transition from tetragonal to cubic phase with a magnetic field at this temperature. Fig. 8c shows that with increasing external field, the AFM moments decrease and the FM moments increase, suggesting the AFM state gradually transforms into the FM state with the increased magnetic field. Even though we cannot achieve complete phase transition from the AFM to the FM state at 140 K under 6 T, the variation of the magnetic state under a magnetic field reflects the close correlation between the magnetic phase transition and the magnetic entropy change in $\text{Mn}_3\text{Cu}_{0.89}\text{N}_{0.96}$. In the tetragonal phase the magneto-crystalline anisotropy may block the transition from tetragonal phase to cubic phase. Thus, it would be interesting to investigate the phase transition from cubic to tetragonal under a magnetic field.

3.5.2. Magnetic field effects at the phase coexistence region (144 K)

Fig. 9a shows the variation in the axes of the tetragonal phase as the magnetic field changes at 144 K. The linear expansion coefficient of a_H and the linear shrinkage coefficient of c_H induced by the magnetic field are 3.73×10^{-5} and $-2.95 \times 10^{-5} \text{ T}^{-1}$, respectively. The volume of the tetragonal phase increases with increasing magnetic field. Fig. 9b and c shows the relations between the unit cell volume, phase fractions and the magnetic field. The variation of magnetism is not shown: as the cubic phase is the dominating phase at 144 K, it is difficult to extract accurate magnetic moment information from the neutron data. As shown in Fig. 9b and c, with increasing magnetic field, the tetragonal phase fraction increases, the tetragonal unit cell volume increases, and the cubic unit cell volume decreases. The total volume ($V = V_T \times F_T + V_c \times F_c$) remains nearly constant at $\sim 59.293 \text{ \AA}^3$ at 144 K. This indicates that the sample is not a homogeneous system, but rather consists of different components with different lattice parameters and transition temperatures. The phase transitions of some components can be induced by a low magnetic field. As the magnetic field changed from 0 to 5 T, the tetragonal fraction increased 5.4% in the current sample with the same trend as that triggered by temperature. This supports the hypothesis that a higher magnetic field may increase the amount of phase transition.

From the present investigations in $\text{Mn}_3\text{Cu}_{0.89}\text{N}_{0.96}$, the structural and the magnetic transitions, as well as the anomalous variation in resistivity, occur within the same region as the two-phase coexistence region. The maximum magnetic entropy change is also within the phase coexistence region. Fig. 7 indicates that the total entropy change is directly related to the structural and magnetic

transitions. The cubic phase corresponds to the PM state and tetragonal phase corresponds to the FIM state. According to the analysis of Figs. 8 and 9, the magnetic field can change the magnetic arrangement (the AFM moments decrease and the FM moments increase) and the phase transition in the tetragonal phase and the two-phase coexistence regions, respectively. The magnetic entropy change is in the temperature range of 135–150 K as shown in Fig. 5b which includes the tetragonal phase and the two-phase coexistence region. This indicates that the magnetic entropy originates partly from the magnetic arrangement change of the tetragonal phase and partly from the phase transition (cubic to tetragonal) induced by the magnetic field. Two Mn atoms have FM moments in the FIM structure of $\text{Mn}_3\text{Cu}_{0.89}\text{N}_{0.96}$. According to the magnetization isotherms in Fig. 5a, the difference in the magnetization between 144 and 146 K is $\Delta M = 4.9193 \text{ emu g}^{-1}$, which corresponds to $\sim 0.207 \mu_B$ per molecule. For the FM component, it is difficult to confirm such tiny changes from NPD refinement. However the variation of AFM and FM moments under a magnetic field at 140 K confirms the presence of the FM moment and the influence of a magnetic field on it. The magnetization is still not saturated under 50 kOe in Fig. 5a, which indicates that the FM component would increase further with the applied magnetic field. Therefore, an even higher magnetic field is needed in order to fully promote a transition from cubic to tetragonal and to achieve a greater magnetic entropy.

Although the total entropy cannot be completely achieved by a 50 kOe magnetic field, the magnetic entropy change of $\text{Mn}_3\text{Cu}_{0.89}\text{N}_{0.96}$ ($13.52 \text{ J kg}^{-1} \text{ K}^{-1}$) is comparable to those of the Gd, $\text{Gd}_5\text{Si}_2\text{Ge}_2$, $\text{Gd}_6\text{Ni}_{3/5}\text{Si}_3$, $\text{MnFeP}_{0.45}\text{As}_{0.55}$, $\text{La}(\text{Fe}_{0.9}\text{Si}_{0.1})_{13}$, MnAs, etc., in which the absolute values of the magnetic entropy change $|\Delta S_m|$ with a field of 50 kOe are $9 \text{ J kg}^{-1} \text{ K}^{-1}$ at 294 K [33], $18 \text{ J kg}^{-1} \text{ K}^{-1}$ at 276 K [33], $5.72 \text{ J kg}^{-1} \text{ K}^{-1}$ [34], $18 \text{ J kg}^{-1} \text{ K}^{-1}$ at 310 K [35], $30 \text{ J kg}^{-1} \text{ K}^{-1}$ at 184 K [36] and $32 \text{ J kg}^{-1} \text{ K}^{-1}$ at 318 K [37], respectively. Although the magnetic entropy change of $\text{Mn}_3\text{Cu}_{0.89}\text{N}_{0.96}$ is not the largest, this could still be a candidate magnetic refrigerant material due to its inexpensive and nontoxic constituent elements, easy preparation, as well as its small M–H hysteresis.

4. Conclusion

In summary, a large entropy change $\sim 60 \text{ J kg}^{-1} \text{ K}^{-1}$ was observed in $\text{Mn}_3\text{Cu}_{0.89}\text{N}_{0.96}$ which originates from phase transitions in this material. This entropy change comprises lattice entropy, electronic entropy and magnetic entropy. The magnetic entropy is $13.52 \text{ J kg}^{-1} \text{ K}^{-1}$ under 50 kOe at 145 K. The magnetic entropy change is caused by (i) the magnetic transition from the AFM to the FM state in the tetragonal phase; and (ii) the phase transition from cubic to tetragonal under a magnetic field. The structural and magnetic transitions and the resistance variations co-occur within the two-phase coexistence region. In the same region, the magnetic field was also observed to be able to

change the phase fraction. These results indicate that the entropy changes in this region induced by the magnetic field comprise not only magnetic entropy but also lattice and electronic entropy. Because of the inexpensive and nontoxic raw materials used and the simple fabrication process involved, the discovery of the MCE in $\text{Mn}_3\text{Cu}_{0.89}\text{N}_{0.96}$ make this material a potential candidate for magnetic refrigerant applications.

Acknowledgements

This work is financially supported by the National Natural Science Foundation of China (NSFC) (Nos. 91122026 and 51172012), the Ph.D. Programs Foundation of Ministry of Education of China (No. 20111102110026) and the China Scholarship Council.

References

- [1] Shen BG, Sun JR, Hu FX, Zhang HW, Cheng ZH. *Adv Mater* 2009;21:4545–64.
- [2] Tohei T, Wada H, Kanomata T. *J Appl Phys* 2003;94:1800–2.
- [3] Yu MH, Lewis LH, Moodenbaugh AR. *J Appl Phys* 2003;93:10128–30.
- [4] Kaneko T, Kanomata T, Miura S, Kido G, Nakagawa Y. *J Magn Mater* 1987;70:261–2.
- [5] Kanomata T, Kikuchi M, Kaneko T, Kamishima K, Bartashevich MI, Katori HA, et al. *Solid State Commun* 1997;101(11):811–4.
- [6] Fruchart D, Bertaut EF. *J Phys Soc Jpn* 1978;44:781–91.
- [7] Yu MH, Lewis LH, Moodenbaugh AR. *J Magn Mater* 2006;299:317–26.
- [8] Lewis LH, Yoder D, Moodenbaugh AR, Fischer DA, Yu MH. *J Phys: Condens Matter* 2006;18:1677–86.
- [9] Tohei T, Wada H, Kanomata T. *J Magn Mater* 2004;272–276:e585–6.
- [10] Iikubo S, Kodama K, Takenaka K, Takagi H, Shamoto S. *Phys Rev B* 2008;77:020409(R).
- [11] Wang BS, Tong P, Sun YP, Luo X, Zhu XB, Li G, et al. *Europhys Lett* 2009;85:47004.
- [12] Shimizu T, Shibayama T, Asano K, Takenaka K. *J Appl Phys* 2012;111:07A903.
- [13] Sun Y, Guo YF, Tsujimoto Y, Wang X, Li J, Sathish CI, et al. *Adv Condens Matter Phys* 2013:286325.
- [14] Chi EO, Kim WS, Hur NH. *Solid State Commun* 2001;120:307–10.
- [15] Ding L, Wang C, Chu LH, Yan J, Na YY, Huang QZ, et al. *Appl Phys Lett* 2011;99:251905.
- [16] Takenaka K, Ozawa A, Shibayama T, Kaneko N, Oe T, Urano C. *Appl Phys Lett* 2011;98:022103.
- [17] Takenaka K, Takagi H. *Appl Phys Lett* 2005;87:261902.
- [18] Huang R, Li L, Cai F, Xu X, Qian L. *Appl Phys Lett* 2008;93:081902.
- [19] Sun Y, Wang C, Wen YC, Zhu KG, Zhao JT. *Appl Phys Lett* 2007;91:231913.
- [20] Iikubo S, Kodama K, Takenaka K, Takagi H, Takigawa M, Shamoto S. *Phys Rev Lett* 2008;101:205901.
- [21] Kodama K, Iikubo S, Takenaka K, Takigawa M, Takagi H, Shamoto S. *Phys Rev B* 2010;81:224419.
- [22] Song X, Sun Z, Huang QZ, Rettenmayr M, Liu X, Seyring M, et al. *Adv Mater* 2011;23(40):02552.
- [23] Wang C, Chu LH, Yao QR, Sun Y, Wu MM, Ding L, et al. *Phys Rev B* 2012;85:220103(R).
- [24] Asano K, Koyama K, Takenaka K. *Appl Phys Lett* 2008;92:161909.
- [25] Shibayama T, Takenaka K. *J Appl Phys* 2011;109:07A928.
- [26] Larson AC, Von Dreele RB. General structure analysis system (GSAS). Los Alamos National Laboratory Report LAUR 86-748; 2004.
- [27] Phan MH, Yu SC. *J Magn Mater* 2007;308:325–40.
- [28] Gschneidner Jr KA, Pecharsky VK, Pecharsky AO, Zimm CB. *Mater Sci Forum* 1999;315–317:69–76.
- [29] Jahn HA, Teller E. *Proc R Soc Lond A* 1937;161:220–35.
- [30] Takenaka K, Shibayama T, Ozawa A, Hamada T, Nakamura T, Kodama K, et al. *J Appl Phys* 2011;110:023909.
- [31] Kamishima K, Bartashevich MI, Goto T, Kikuchi M, Kanomata T. *J Phys Soc Jpn* 1998;67:1748–54.
- [32] Jardin J-P, Labbe J. *J Solid State Chem* 1983;46:275–93.
- [33] Pecharsky VK, Gschneidner Jr KA. *Phys Rev Lett* 1997;78:4494–7.
- [34] Gaudin E, Tencé S, Weill F, Fernandez JR, Chevalier B. *Chem Mater* 2008;20:2972–9.
- [35] Tegus O, Brück E, Buschow KHJ, de Boer FR. *Nature* 2002;415:150–2.
- [36] Fujita A, Fujieda S, Hasegawa Y, Fukamichi K. *Phys Rev B* 2003;67:104416.
- [37] Wada H, Tanabe Y. *Appl Phys Lett* 2001;79:3302–4.